Heterogeneously Integrated Membrane Lasers on Si Substrate for Low Operating Energy Optical Links

Takuro Fujii , Koji Takeda , *Senior Member, IEEE*, Nikolaos-Panteleimon Diamantopoulos , *Member, OSA*,
Erina Kanno, Koichi Hasebe, *Member, OSA*, Hidetaka Nishi, *Member, OSA*, Ryo Nakao ,
Takaaki Kakitsuka, *Member, IEEE*, and Shinji Matsuo , *Fellow, IEEE*

(Invited Paper)

Abstract—High demand exists for low operating energy optical links that use wavelength division multiplexing technologies in datacenter networks. Thus, we fabricate a directly modulated membrane distributed-reflector laser with low operating energy on a thermally oxidized silicon (Si) substrate. Because we use epitaxial growth to bury an active region on a directly bonded InP-based membrane, it needs to be kept within a critical thickness, which is related to the growth temperature and the thermal expansion coefficients of materials. In previous studies, we used 250-nm-thick structures, causing relatively large series resistance that limited device performance on such aspects as energy cost and output power. In this study, we increase the III–V membrane thickness to 350 nm, which is close to the calculated critical thicknesses. We achieve the same high crystal quality of multiquantum-wells found in our previous studies. The fabricated laser shows a differential resistance of 72 Ω and thermal resistance of 982 K/W. Thanks to a reduction in bias voltage, the laser can be directly modulated at 25.8 Gbit/s with an energy cost of 97 fJ/bit. In addition, due to a reduction in heat generation, direct modulation with a 50-Gbit/s non return to zero signal is demonstrated by increasing bias current up to 10 mA.

Index Terms—Epitaxial growth, quantum well lasers, semiconductor lasers, wafer bonding.

I. INTRODUCTION

THE rapid increase in transmission capacity and power consumption in data centers are becoming big issues [1]. Therefore, large-capacity, low-power consumption, and low-cost optical links are desired for datacenters. Currently, vertical-cavity surface-emitting lasers (VCSELs) are widely used in these networks because they offer 25-Gbit/s or faster direct modulation with a low-energy cost of around 100 fJ/bit [2]–[5].

However, using single mode fibers with dense-wavelength division multiplexing (DWDM) technologies is a challenge. This is because VCSELs use a wavelength-scale cavity to improve the modulation efficiency, so the lasing wavelength is sensitive to its cavity length, which makes precise control of the lasing wavelength difficult [5]. In contrast, in-plane InP-based distributed-feedback (DFB) lasers are widely used in metro- and long-haul WDM networks because they satisfy requirements such as wavelength controllability and single-mode operation [6]–[8]. However, the energy cost of DFB lasers is almost ten-times higher than that of VCSELs because they need relatively large active volume due to the smaller coupling coefficient of the grating, i.e., large mirror loss, compared with VCSELs.

Another important issue is the cost because datacom applications require a huge number of transmitters. Large-scale photonic integrated circuits (PICs) have attracted much attention in efforts to reduce the fabrication and assembly costs. In this context, processing heterogeneously-integrated III–V materials on a large-scale silicon wafer are a promising solution because of a size limitation in the InP wafer [9], [10].

To overcome these problems, we have been developing DFB and distributed-reflector (DR) lasers with a membrane structure integrated on a thermally oxidized silicon wafer (SiO$_2$/Si wafer) [11]–[14]. A membrane InP-based structure sandwiched between low-refractive-index materials enables increasing the grating-index coupling coefficient (κ), resulting in small mirror loss of the cavity. This structure also enables a stronger optical confinement factor compared to conventional InP buried heterostructure (BH) lasers. Therefore, high modulation efficiency and very low energy consumption can be achieved using a DWDM-adaptive DFB cavity structure [14]–[16].

In our fabrication scheme, the InP-based layers including InGaAsP-based multi-quantum wells (MQWs) are directly bonded to a SiO$_2$/Si substrate. All fabrication processes including epitaxial regrowth of InP are carried out on SiO$_2$/Si substrate, so we have to find a way to overcome the problem caused from the difference in the thermal expansion coefficients of InP, SiO$_2$, and Si. The key to achieving the proposed process is controlling the InP-based layer thickness to less than its critical thickness because we have to suppress the degradation in the epitaxial layer during high-temperature processes such as epitaxial regrowth and selective doping [13]. These aspects make
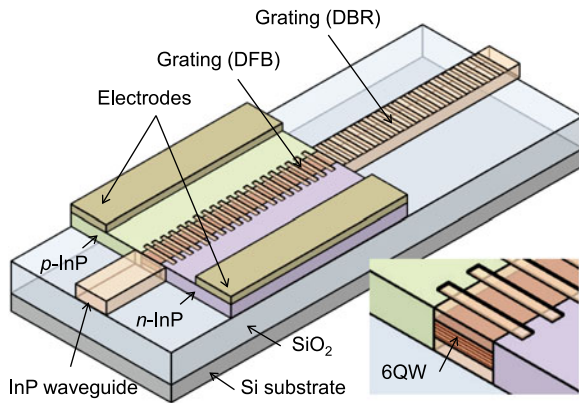
Fig. 1.   Schematic of membrane DR laser integrated on SiO$_2$.

the membrane laser a promising candidate for light sources in datacom networks.

In previous studies, we developed membrane DFB and DR lasers with a 250-nm-thick III–V layer [11]–[14]. The fabricated 50-μm-long membrane DR laser shows a 25.8-Gbit/s direct modulation with non-return to zero (NRZ) signal at an energy cost of 132 fJ/bit [14]. To the best of our knowledge, this is the most energy-efficient in-plane DFB or DR laser reported so far. However, a thin membrane structure integrated on SiO$_2$ results in high series and thermal resistance. Consequently, device performance regarding aspects such as output power and modulation speed are restricted because we cannot increase the current density due to the increase in the active region temperature. Moreover, the series resistance has a direct effect on the power consumption and energy cost of laser operation.

In this paper, we describe the fabrication of a membrane DR laser that has a 350-nm-thick structure. A thicker membrane compared with our previously developed lasers provides low electrical and thermal resistance. Thus, we expect to achieve a reduction in energy cost and the suppression of the temperature increase in the active region at a higher bias current density. A 350-nm-thick InP-based active layer is directly bonded to the SiO$_2$/Si substrate, and the crystal quality after the high temperature process was confirmed using photoluminescence (PL) and x-ray diffraction (XRD) measurements. The fabricated DR laser exhibited a threshold current of 0.77 mA, and a differential resistance of less than 72 Ω when the bias current was 10 mA. A reduction in temperature increase per injection current due to a thicker membrane structure was successfully confirmed. We achieved an energy cost of 97 fJ/bit for 25.8-Gbit/s NRZ direct modulation, and we also demonstrated NRZ direct modulation at 40- and 50-Gbit/s.

II. DESIGN AND FABRICATION OF MEMBRANE LASER

Fig. 1 shows a schematic of a membrane DR laser on a SiO$_2$/Si substrate. The 350-nm-thick epitaxial III–V layers consist of a 6-period MQW stack ($\sim$105 nm) sandwiched between an underlying InP layer ($\sim$165 nm) and InP cap layer ($\sim$80 nm). The III–V layer is integrated on a 2-inch Si substrate with 2-μm-thick thermal oxide. The active core is InGaAsP/InP BH with a width

of 1.0 μm and a length of 75 μm. The InP cap layer is periodically etched to form a surface grating that determines the lasing wavelength. The cavity consists of a 75-μm-long DFB section and a 50-μm-long distributed Bragg reflector (DBR) section. Because we use a high grating-index coupling coefficient (κ) to achieve low operating energy, we use a uniform grating for the DFB section to suppress spatial hole burning compared with when using a λ/4-shifted grating. A stable single-mode lasing is achieved by selective reflection of one of the stopband-edges of the DFB cavity using a DBR mirror. This structure also enables us to achieve selective optical output from the front-side waveguide.

The total thickness of the III–V layer should be determined by the crystal quality. During the epitaxial regrowth of InP to bury an active region, the directly bonded wafer is exposed to a temperature of around 600 °C. This induces a significant amount of thermal strain caused by the difference in thermal expansion coefficients between InP and Si. The thermal strain at growth temperature ($\sim$600 °C) was calculated to be approximately 800 ppm, corresponding to the calculated critical thickness of between 200 nm (mechanical equilibrium model) and 430 nm (energy equilibrium model) [13]. The experimental results also confirmed this calculation; we observed the line-defect in a directly-bonded 500-nm-thick InP-based membrane after exposing the regrowth condition, while neither line- nor point-defects were observed for a 250-nm-thick one [13]. On the basis of that, previously we designed the III–V membrane thickness of DFB and DR lasers to be 250 nm [11]–[14].

However, the thin membrane structure results in high-series resistance because the membrane lasers use lateral current injection. A high series resistance induces a temperature increase in the active region that causes degradation in gain. Therefore, we evaluated the high-temperature tolerance of a thicker InP-based membrane directly bonded to a SiO$_2$/Si wafer. We set the total thickness at 350 nm, which is 100-nm thicker than our previous design. The wafer was annealed at 600 °C for 30 min in a metalorganic vapor phase epitaxy (MOVPE) reactor. The crystal-quality characterization was carried out before and after annealing. Fig. 2 compares the PL spectra for 6QWs before and after annealing. The same-structure MQWs grown on the InP substrate is also shown as a reference. The excitation light is a continuous-wave operation laser diode at a wavelength of 980 nm. The characterization in the PL intensity was carried out by comparing the median value of all measured points except where the voids appear. The PL intensity was $\sim$5 times greater for the MQWs on SiO$_2$ than for those on InP. This seems to occur because both the excitation and collection efficiencies were enhanced due to underlying InP/SiO$_2$ and SiO$_2$/Si interfaces. The change in PL intensity after annealing was only 6%. In addition, no change was observed in the spectral shapes or peak wavelength. We also evaluated a micro-scale PL-intensity distribution using a focused-laser beam at a wavelength of 1064 nm. Fig. 3 shows a peak-intensity map after annealing. We found no significant dark lines or spots over 500 μm $\times$ 500 μm. Fig. 4 compares the (004) diffraction peaks for MQWs on SiO$_2$/Si, before and after annealing, with XRD ω-2θ scans. We simultaneously observed the peaks close to ω = 31.67 degrees and
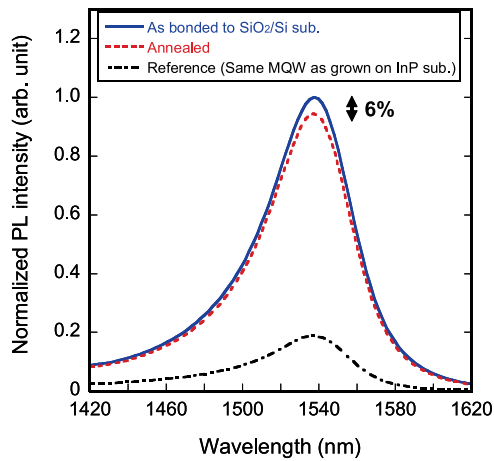
Fig. 2. PL spectra for MQWs on SiO$_2$/Si wafer before (blue solid line) and after (red dashed line) annealing, compared with the same MQWs grown on InP substrate (black dashed line).
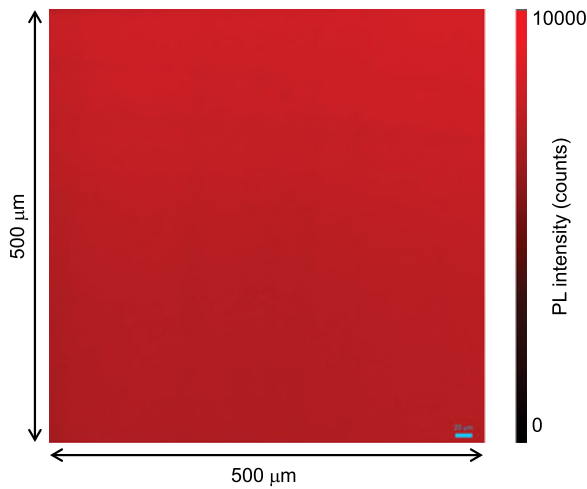

Fig. 3. Micro-scale PL intensity map (500 μm $\times$ 500 μm) for MQWs on SiO$_2$/Si wafer.

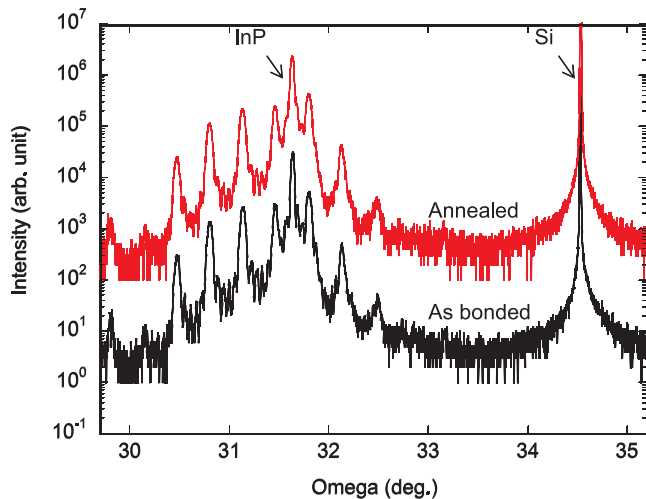Fig. 4. XRD ω-2θ characteristics of 350-nm-thick InP-based membrane that includes MQWs before and after exposure to MOVPE regrowth condition.
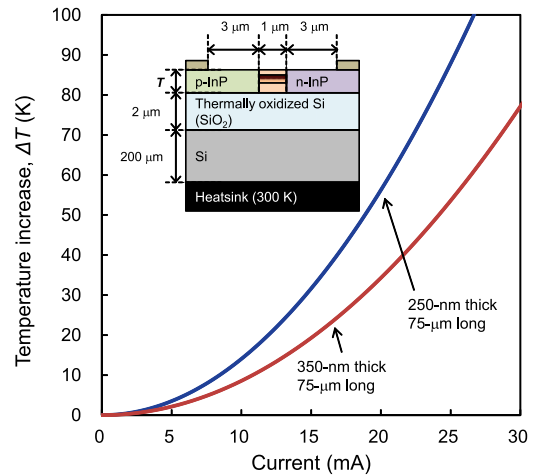

Fig. 5. Estimated temperature increase in InGaAsP active core as a function of injection current. The inset shows calculation model for the temperature increase in the InGaAsP core.

34.56 degrees, corresponding to the lattice constant of InP and Si, respectively. The satellite peaks mainly represent the strain, thickness, interfacial-steepness and number of quantum wells. We did not observe any significant change in the position or width of the peaks. These measurements revealed that the MQWs' structure remains almost the same even when the directly-bonded wafer is exposed to an MOVPE regrowth condition, when the total thickness of the III–V layer is 350 nm.

We then estimated the effect of thickening the InP-based membrane on the temperature increase. We carried out a 2-dimensional thermal diffusion calculation using the cross section shown in Fig. 5. We assumed that only the Joule heat contributes as the heat source in the n- and p-clad regions due to the lateral current between the contact layer edges and active region edges. Therefore, the resistance in the clad regions is inversely proportional to the layer thickness. The doping density in the p- and n-regions is $1 \times 10^{18} \, \text{cm}^{-3}$. The resistivity in n- and p-clad regions is $1.1 \times 10^{-3} \, \Omega \cdot \text{cm}$ and $4.2 \times 10^{-2} \, \Omega \cdot \text{cm}$, respectively. The Dirichlet boundary condition was set at the bottom of the silicon substrate. Fig. 5 shows a calculated temperature increase in the active region as a function of injection current. The temperature increase at the same injection current is 39% lower when the membrane is thickened from 250 nm to 350 nm. This enables increasing the current injection so that higher output power and relaxation oscillation frequency can be achieved. The increase in III–V thickness causes a decrease in the optical confinement factor when the QW structure is the same. Fig. 6 compares the calculated optical mode-field in QWs when the total thickness is 250 nm and 350 nm. This figure also shows the optical mode-field for a conventional InP-based BH laser that includes 1.8-μm-wide 6QWs and a 100-nm-thick separate confinement heterostructure. The optical confinement factor for 6QWs in a 350-nm-thick membrane structure is 10.1% while that in a 250-nm-thick structure is 12.4%. However, 10.1% confinement is still approximately 1.7 times greater than that in conventional InP-based BH lasers.
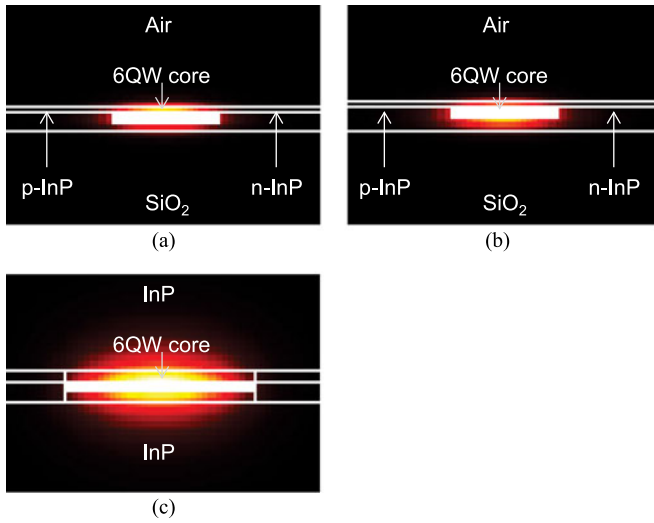
Fig. 6. Calculated optical mode-field of BH (a) 250-nm-thick membrane integrated on SiO$_2$. (b) 350-nm-thick membrane integrated on SiO$_2$. (c) Conventional InP-based MQW laser.

We then fabricated the membrane DR laser with the 350-nm-thick III–V structure. Fig. 7 shows the fabrication procedure. First, an etch-stop InGaAs layer and a 350-nm-thick InP-based membrane layer that consists of a ∼105 nm active core sandwiched between InP layers were grown on a 2-inch InP (001) wafer. The active core has 6-period InGaAsP-based MQWs. Next, the epitaxial InP wafer was bonded to a 2-inch SiO$_2$/Si (001) wafer with a 2-μm-thick thermal oxide layer. Then, the epitaxial InP-based membrane layer was left on the SiO$_2$/Si wafer by mechanical polishing and chemical etching of the native InP substrate. After that, we deposited a selective etching mask on the InP membrane and defined mesa-stripes using dry and wet etching. This process leaves a 175-nm-thick InP layer except for the region where the etching mask was formed. And then, we selectively regrew an undoped InP layer using the MOVPE to fabricate a InGaAsP/InP BH. After that, we fabricated a lateral p-i-n junction by means of thermal diffusion of Zn for p-type doping and ion implantation of Si for n-type doping. Then, surface gratings were formed by dry etching of InP. The grating pitches were different between the DFB section (above the active region) and the DBR section (on the rear-side of active region). After that, the InP waveguide was formed by dry etching. The excess InP-based layers were also removed here. The InP waveguide was taper-terminated to suppress the back reflection. Finally, Au-based electrodes were deposited on both the p- and n- doped InP regions to form an electrical contact.

III. DEVICE CHARACTERISTICS

A. Static Characteristics

Static characteristics measurements were carried out by detecting light output from the InP waveguide edge using an optical power meter. Fig. 8 shows the optical output power and the bias current versus the injection current (L-I-V characteristics) at room temperature (RT). It also shows the characteristics for a
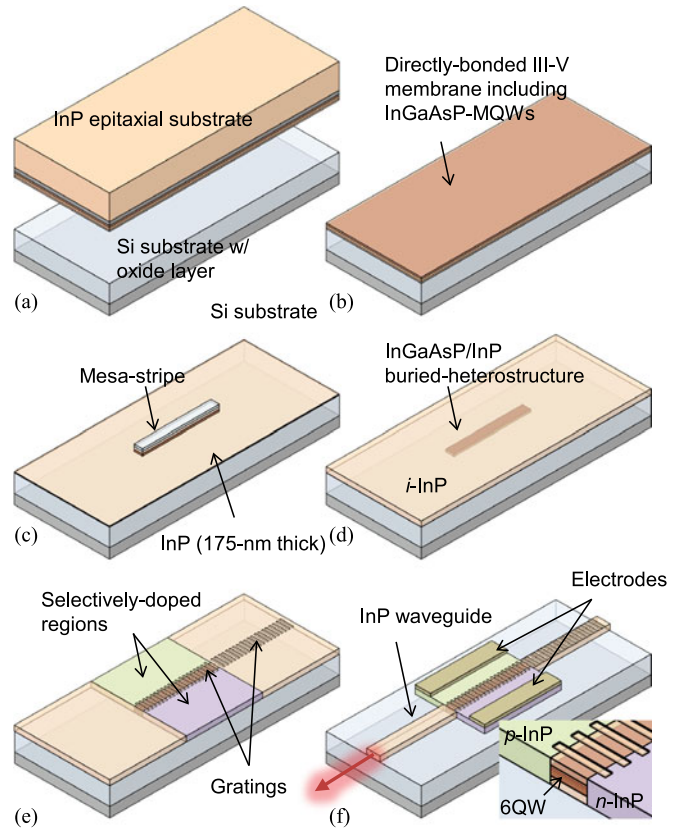

Fig. 7. Fabrication procedure for membrane DR lasers on SiO$_2$/Si substrate. (a) Direct bonding of InGaAsP-based active layer and InGaAs etchstop layer grown on InP substrate to SiO$_2$/Si substrate. (b) Removal of InP substrate. (c) Formation of mesa-stripe that leaves 170-nm-thick InP-membrane on SiO$_2$. (d) Epitaxial regrowth of InP to fabricate InGaAsP/InP BH. (e) Formation of p-i-n junction and gratings. (f) Formation of InP waveguides and electrodes.
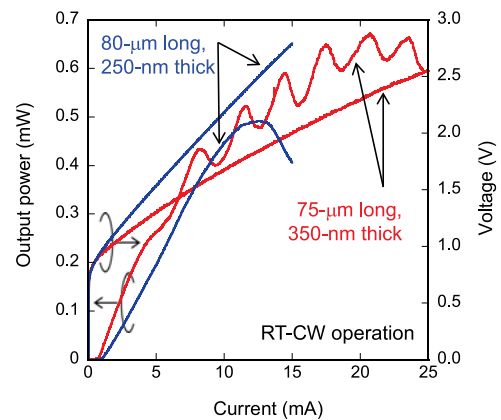

Fig. 8. Dependence on bias current of optical output power and bias voltage (L-I-V characteristics) for developed 350-nm-thick laser and previous 250-nm-thick device.

previously developed 250-nm-thick and 80-μm-long DR laser. They had the same-structure InGaAsP-6QWs as an active core and were integrated on 2-μm-thick SiO$_2$, so the device structures are very similar except for their total thickness. The kinks at a high bias current seem to be caused because of reflections from
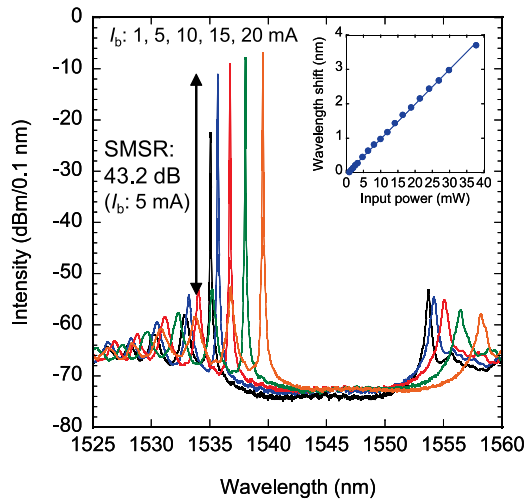
Fig. 9. Lasing spectra of DR lasers at RT when a bias current is increased from 1 mA to 20 mA. The inset shows wavelength shift as a function of input power.
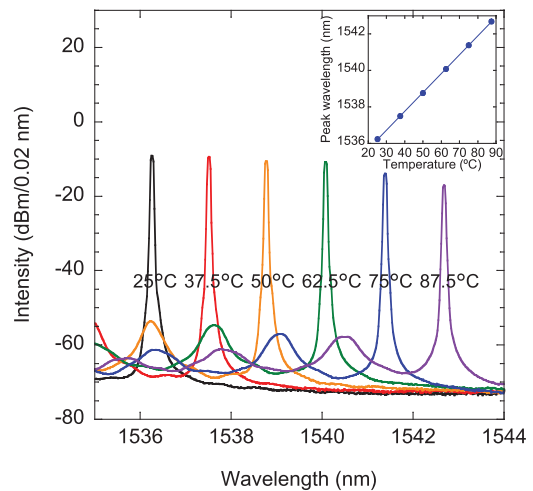

Fig. 10. Lasing spectra of DR lasers at a bias current of 8 mA when the temperature is controlled from 25 °C to 87.5 °C. The inset shows the dependence on temperature of the lasing wavelength.

the InP-waveguide edge due to lack of anti-reflection coating or an integrated spot-size convertor (SSC) [14]. The 350-nm-thick laser exhibited a threshold current of 0.77 mA, and a differential resistance of 72 Ω when the bias current was 10 mA. Due to the thicker membrane structure, the differential resistance for the 350-nm-thick laser is approximately 42% lower than that for the 250-nm-thick one. In addition, an injection current at which the maximum output power was observed increases from 13 mA to 22 mA. No significant change occurred in the threshold current, indicating that the crystal quality remains the same, even though we used a 100-nm-thicker structure.

Next, we measured the bias-current dependence of the lasing wavelength and temperature dependence of the lasing wavelength, revealing the temperature change at a certain injection current. Fig. 9 shows the lasing spectra of a 350-nm-thick laser at bias currents of 1, 5, 10, 15 and 20 mA. We observed single-mode lasing at wavelengths from 1535 to 1540 nm. The side-mode suppression ratio was 44.0 dB when the bias current was 10 mA. Although the ripples observed on the bottom of the stop-band indicate external optical feedback due to reflections, the shorter wavelength edge of the DFB stopband was successfully selected at any injection current by the DBR mirror and no mode hopping was observed. We estimated the grating index coupling coefficient at $\sim 1000 \, \mathrm{cm}^{-1}$ from the DFB stopband width of 18.4 nm. The inset shows a wavelength shift as a function of input electrical power. The slope, $\Delta\lambda/\Delta P$, was 0.101 nm/mW. Fig. 10 also shows the lasing spectra. Here, we used a bias current of 8 mA and controlled the stage temperature from 25 °C to 87.5 °C. The inset shows a wavelength shift as a function of temperature change. The slope, $\Delta\lambda/\Delta T$, was 0.103 nm/K. The calculated thermal resistance was 982 K/W, which was 49% suppressed compared to a 250-nm-thick and 50-μm-long device and 28% suppressed compared to 250-nm-thick and 80-μm-long devices [14]. Fig. 11 shows the lasing wavelength shift and the corresponding temperature change calculated from $\Delta\lambda/\Delta T$ as a function of the bias current. We compared the
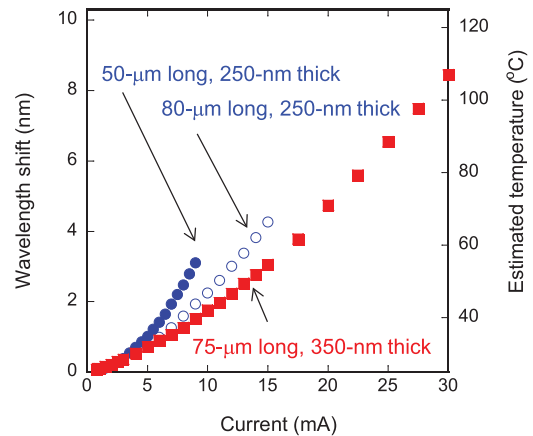

Fig. 11. Shift in lasing wavelength of DR lasers and corresponding active-core temperature versus bias current.

currently developed device and previously developed 250-nm-thick devices. The temperature increase in the 350-nm-thick membrane structure with a 75-μm-long active region was 52% suppressed from a 50-μm-long device and was 30% suppressed from an 80-μm-long device, due to a reduction in differential resistance.

B. Dynamic Characteristics

We then evaluated the dynamic characteristics of the 350-nm-thick membrane DR laser. Fig. 12 shows the relaxation oscillation frequency, f_{r}, as a function of the square root of the bias current above the threshold at RT. We measured the relative intensity noise (RIN) to evaluate f_{r}. The modulation efficiency was 9.1 GHz/mA$^{1/2}$, which is almost the same as that of a previously developed laser, even though the active volume is 1.5-times greater. Assuming that the maximum modulation speed is calculated as $1.3 \times 1.55 \times f_{\mathrm{r}}$, a 25.8 Gbit/s
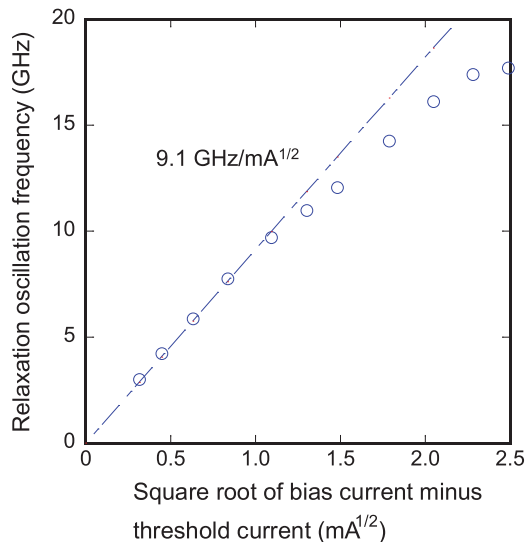
Fig. 12. Relaxation oscillation frequency as a function of the square root of the bias current above the threshold.

TABLE I
OPERATING CONDITIONS FOR DIRECT MODULATION

	25.8 Gbit/s (a)	25.8 Gbit/s (b)	40 Gbit/s (c)	50 Gbit/s (d)
I_b	2.4 mA	3.0 mA	9.0 mA	10.0 mA
V_b	1.04 V	1.10 V	1.56 V	1.64 V
V_{p-p}	0.130 V	0.190 V	0.759 V	0.791 V
Energy cost	97 fJ/bit	128 fJ/bit	351 fJ/bit	328 fJ/bit

direct modulation with an injection current of 2.7 mA would be expected [17], [18].

Next, we demonstrated a direct modulation with a NRZ signal having a modulation speed of up to 50 Gbit/s. The measurement was carried out at RT, and a $2^{31}-1$ pseudo-random bit sequence (PRBS) was used. Fig. 13 shows the measured eye diagrams for 25.8, 40, and 50 Gbit/s monitored with a digital sampling oscilloscope. The bias current, I_b, bias voltage, V_b and voltage swing, V_{p-p} are listed in Table I. The energy costs were calculated by dividing the applied DC energy by the bit rate, which is commonly used to qualify the power consumption of VCSELs [2]. We observed an eye-opening at a modulation speed of 25.8 Gbit/s when the bias current was >2.4 mA. Thanks to a reduction in bias voltage, the corresponding energy costs were 97 fJ/bit (I_b: 2.4 mA) and 128 fJ/bit (I_b: 3.0 mA). To the best of our knowledge, this is the most energy-efficient DR or DFB laser reported that we are aware of. In addition, a reduction in temperature increase enables us to increase a bias current, so a 40- and 50-Gbit/s direct modulation was also demonstrated. We observed an eye-opening for 40 Gbit/s with an energy cost of 351 fJ/bit (I_b: 9.0 mA). Further improvement in modulation speed and output power would be possible by increasing the internal quantum efficiency, which is estimated to be 32.4% [19], which is lower than the maximum achievable value of ~70%. Optimizing the epitaxial layer structure such as by increasing the number of QWs seems a promising way to achieve efficient current
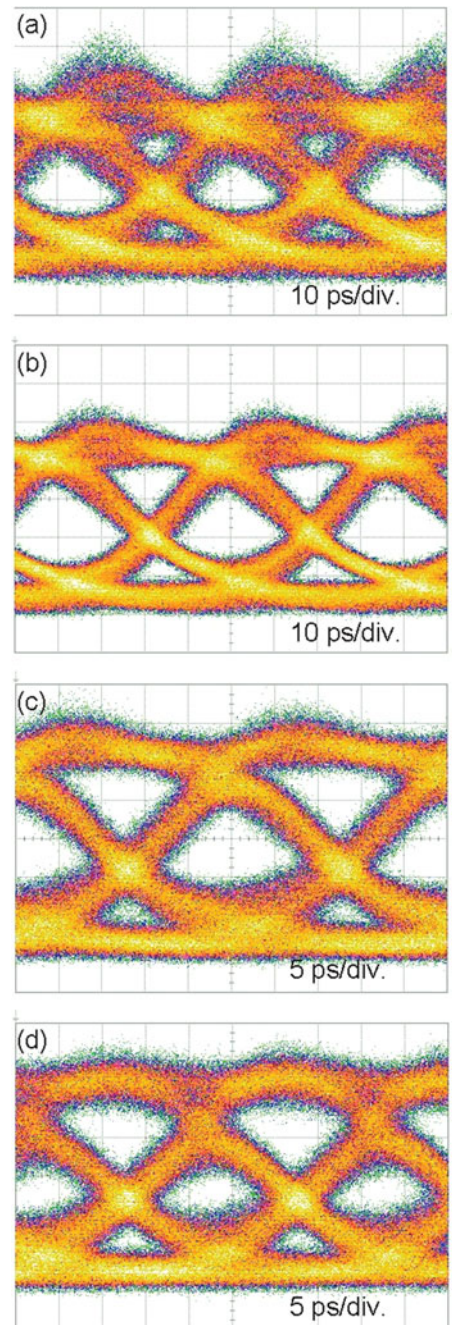

Fig. 13. Eye diagrams for membrane DR lasers directly modulated at (a, b) 25.8 Gbit/s (c) 40 Gbit/s and (d) 50 Gbit/s. The zero-points are at the bottom of the figures.

injection. The integration of SSC is also promising to increase both static and dynamic characteristics because the SSC provides low-loss coupling to single-mode fibers, and it also suppresses the unexpected external optical feedback due to the reflection [14].

IV. CONCLUSION

We developed a membrane DR laser on a SiO$_2$/Si wafer that has a 350-nm-thick III–V membrane layer. We designed this

relatively thick membrane structure to reduce the series resistance so that temperature increases would be suppressed. Because a 350 nm is close to, or even greater than the calculated critical thickness of directly-bonded InP on Si at an MOVPE growth temperature (∼600 °C), we systematically determined that the crystal quality of InGaAsP-based 6QWs remains almost the same even after exposing the directly-bonded wafer to an MOVPE regrowth condition. Thanks to the 100-nm-thicker membrane structure, we successfully achieved a reduction in differential resistance and an increase in temperature. The fabricated DR laser exhibited a 25.8-Gbit/s direct modulation with a low energy cost of 97 fJ/bit, and we also demonstrated 40- and 50-Gbit/s direct modulation. These results demonstrate that our laser is promising for future network applications in data centers and the proposed fabrication procedure is a promising way to fabricate InP-based large-scale PICs.

ACKNOWLEDGMENT

REFERENCES

[1] Cisco, "Cisco global cloud index: Forecast and methodology, 2015–2020," 2016. [Online]. Available: http://www.cisco.com/c/en/us/solutions/collateral/service-provider/global-cloud-index-gci/Cloud_Index_White_Paper.html

[2] P. Moser *et al.*, "56 fJ dissipated energy per bit of oxide-confined 850 nm VCSELs operating at 25 Gbit/s," *Electron. Let.*, vol. 48, no. 20, 1292–1294, Sep. 2012.

[3] A. Larsson *et al.*, "30 GHz bandwidth 850 nm VCSEL with sub-100 fJ/bit energy dissipation at 25–50 Gbit/s," *Electron. Lett.*, vol. 51, no. 14, pp. 1096–1098, Jul. 2015.

[4] D. M. Kuchta *et al.*, "A 50 Gb/s NRZ modulated 850 nm VCSEL transmitter operating error free to 90 °C," *J. Lightw. Technol.*, vol. 33, no. 4, pp. 802–810, Feb. 2015.

[5] C. Xie *et al.*, "400-Gb/s PDM-4PAM WDM system using a monolithic 2 × 4 VCSEL array and coherent detection," *J. Lightw. Technol.*, vol. 33, no. 3, pp. 670–677, Feb. 2015.

[6] W. Kobayashi *et al.*, "50-Gb/s direct modulation of 1.3-μm InGaAlAs-based DFB laser with ridge waveguide structure," *IEEE J. Sel. Topics Quantum Electron.*, vol. 19, no.4, Jul./Aug. 2013, Art. no. 1500908.

[7] K. Nakahara *et al.*, "Direct modulation at 56 and 50 Gb/s of 1.3-μm InGaAlAs ridge-shaped-BH DFB lasers," *IEEE Photon. Technol. Lett.*, vol. 27, no. 5, pp. 535–536, Mar. 2015.

[8] Y. Matsui *et al.*, "28-Gbaud PAM4 and 56-Gb/s NRZ performance comparison using 1310-nm Al-BH DFB Laser," *J. Light. Technol.*, vol. 34, no. 11, pp. 2677–2683, Jun. 2016.

[9] S. R. Jain, M. N. Sysak, G. Kurczveil, and J. E. Bowers, "Integrated hybrid silicon DFB laser-EAM array using quantum well intermixing," *Opt. Express*, vol. 19, no. 14, pp. 13692–13699, Jul. 2011.

[10] A. Abbasi *et al.*, "High speed direct modulation of a heterogeneously integrated InP/SOI DFB laser," *J. Lightw. Technol.*, vol. 34, no. 8, pp. 1683–1687, Apr. 2016.

[11] S. Matsuo *et al.*, "Directly modulated buried heterostructure DFB laser on SiO_2/Si substrate fabricated by regrowth of InP using bonded active layer," *Opt. Express*, vol. 22, no. 10, pp. 12139–12147, May 2014.

[12] S. Matsuo *et al.*, "Directly modulated DFB laser on SiO_2/Si substrate for datacenter networks," *J. Lightw. Technol.*, vol. 33, no. 6, pp. 1217–1222, Mar. 2015.

[13] T. Fujii *et al.*, "Epitaxial growth of InP to bury directly bonded thin active layer on SiO_2/Si substrate for fabricating distributed feedback lasers on silicon," *IET Optoelectron.*, vol. 9, no. 4, pp. 151–157, Aug. 2015.

[14] H. Nishi *et al.*, "Membrane distributed-reflector laser integrated with SiO_x-based spot-size converter on Si substrate," *Opt. Express*, vol. 24, no. 16, pp. 18346–18352, Aug. 2016.

[15] T. Okamoto *et al.*, "Optically pumped membrane BH-DFB lasers for low-threshold and single-mode operation," *IEEE J. Sel. Topics Quantum Electron.*, vol. 9, no. 5, pp. 1361–1366, Sep./Oct. 2003.

[16] D. Inoue *et al.*, "Low-bias current 10 Gbit/s direct modulation of GaInAsP/InP membrane DFB laser on silicon," *Opt. Express*, vol. 24, no. 16, pp. 18571–18579, Aug. 2016.

[17] R. S. Tucker, J. M. Wiesenfeld, P. M. Downey, and J. E. Bowers, "Propagation delays and transition times in pulse modulated semiconductor lasers," *Appl. Phys. Lett.*, vol. 48, pp. 1707–1709, Apr. 1986.

[18] L. A. Coldren, S. W. Corzine, and M. L. Mashanovitch, *Diode Lasers and Photonic Integrated Circuits*, 2nd ed. Hoboken, NJ, USA: Wiley, 2012.

[19] T. Fujii *et al.*, "Evaluation of device parameters for membrane lasers on Si fabricated with active-layer bonding followed by epitaxial growth," *IEICE Trans. Electron.*, vol. E100-C, no. 2, pp. 196–203, Feb. 2017.

Takuro Fujii was born in Kyoto, Japan, in 1986. He received the B.E. and M.E. degrees in system design engineering from Keio University, Kanagawa, Japan, in 2010 and 2012.

In 2012, he joined NTT Photonics Laboratories, Atsugi, Japan. He has been researching MOVPE growth of III–V semiconductors and the development of III–V semiconductor lasers on Si for photonic integrated circuits.

He is a member of Institute of Electronics, Information and Communication Engineers (IEICE) and Japanese Society of Applied Physics (JSAP). He is the recipient of the Young Scientist Presentation Award from the JSAP in 2014.

Koji Takeda (S'06–M'10–SM'16) received the B.S., M.S., and Ph.D. degrees in electronics engineering from the University of Tokyo, Tokyo, Japan, in 2005, 2007, and 2010, respectively.

From 2008 to 2010, he received research fellowship for young scientists from Japan Society for the Promotion of Science. In 2010, he joined NTT Photonics Laboratories. His current research interests include ultralow-power optical interconnect, InP photonic integrated circuit, and photonic crystal lasers.

He is a member of the IEICE and the JSAP. He is the recipient of the Best Student Paper Award from IEEE Photonics Society in 2009 and the Outstanding Student Presentation Award from JSAP in 2010.

Nikolaos-Panteleimon Diamantopoulos was born in Athens, Greece, in 1988. He received the B.Sc. degree from the University of Peloponnese, Tripoli, Greece, in 2009, the double M.Sc. degree from Aston University, Birmingham, U.K., and Scuola Superiore Sant'Anna Pisa, Pisa, Italy, in 2012, and the Ph.D. degree in information and communications technology from Osaka University, Suita, Japan, in 2016. He has also worked under several EU R&D projects at Athens Information Technology (AIT) Center, Greece, from 2011 to 2016.

In 2016, he joined NTT Device Technology Laboratories, Atsugi, Japan. His current research interests include digital processing techniques for direct-detected optical communication systems and photonic integrated circuits.

Erina Kanno was born in Hokkaido, Japan, in 1989. She received the B.S. degree from Aoyama Gakuin University, Tokyo, Japan, in 2012 and the M.S. degree from the University of Tokyo, Tokyo, Japan, in 2014.

In 2014, she joined NTT Photonics Laboratories, Atsugi, Japan, in 2014. She has been researching ultralow-power consumption optical devices, including short-cavity lasers on Si.
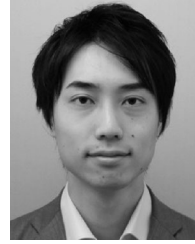
Ryo Nakao was born in Tottori, Japan, in 1987. He received the B.E. and M.E. degrees in electrical, electronic, and information engineering from Osaka University, Suita, Japan, in 2010 and 2012.

He joined NTT Photonics Laboratories, Atsugi, Japan, in 2012. His research interests include the MOVPE growth of III–V semiconductors and the development of semiconductor lasers.

He is a member of JSAP.

Koichi Hasebe was born in Tochigi, Japan, in 1981. He received the M.E. and Ph.D. degrees in electronics and applied physics from Tokyo Institute of Technology, Tokyo, Japan, in 2005 and 2008. He received a research fellowship for young scientists from the Japan Society for the Promotion of Science for the years 2006–2009. In 2008, he was a Postdoctoral Fellow and Visiting Researcher with Tokyo Institute of Technology and the University of California, Berkeley, CA, USA.

Since 2009, he has been with NTT Photonics Laboratories, Atsugi, Japan. His current research interests include next-generation access systems, InP photonic functional devices, and nanomicrocavity semiconductor lasers.

He is a member of the IEICE and Optical Society of America.

Takaaki Kakitsuka (M'11) was born in Kumamoto, Japan, in 1971. He received the B.S. and M.S. degrees in physics and the Dr. Eng. Degree from Kyushu University, Fukuoka, Japan, in 1994, 1996, and 2012, respectively.

In 1996, he joined the NTT Optoelectronics Laboratories, Nippon Telegraph and Telephone Corporation, Kanagawa, Japan. He has been involved in research on semiconductor lasers and optical functional devices. From 2009 to 2011, he was a member of Research and Development Planning Department. He is currently with the NTT Device Technology Laboratories, Atsugi, Japan.

He is a member of the IEICE, the JSAP, and the Physical Society of Japan.

Hidetaka Nishi received the B.S. and M.S. degrees in mechanical science and engineering and the Ph.D. degree from Tokyo Institute of Technology, Tokyo, Japan, in 2005, 2007, and 2016, respectively.

In 2007, he joined NTT Microsystem Integration Laboratories. Since then, he has been conducting research on integrated silicon photonic devices.

He is a member of the Optical Society of America and JSAP.

Shinji Matsuo (M'95–SM'14–F'16) received the B.E. and M.E. degrees in electrical engineering from Hiroshima University, Higashihiroshima, Japan, in 1986 and 1988, and the Ph.D. degree in electronics and applied physics from Tokyo Institute of Technology, Tokyo, Japan, in 2008.

In 1988, he joined NTT Optoelectronics Laboratories, where he researched photonic functional devices using multiple quantum well pin modulators and VCSELs. In 1997, he researched optical networks using WDM technologies at NTT Network Innovation Laboratories. Since 2000, he has been researching high-speed tunable optical filters and lasers at NTT Photonics Laboratories, Atsugi, Japan, and NTT Device Technology Laboratories, Atsugi, Japan.

He is a Senior Distinguished Researcher with NTT. He is a member of the JSAP and IEICE.